DNA damage induces senescent phenotypes in mouse NIT1 beta cells and human islets

Gabriel Brawerman[1,2] and Peter J. Thompson[3,4,5]

[1]Department of Physiology and Pathophysiology, Rady Faculty of Health Sciences, University of Manitoba

[2]Children's Hospital Research Institute of Manitoba, Winnipeg, MB R3E 3P4, Canada

[3]Diabetes Center, University of California San Francisco, San Francisco, CA 94143 USA

[4]Current address and affiliation: Department of Physiology and Pathophysiology, Rady Faculty of Health Sciences University of Manitoba, Children's Hospital Research Institute of Manitoba, Winnipeg, MB R3E 3P4, Canada

[5]Corresponding author: peter.thompson@umanitoba.ca

Pancreatic beta cells are essential endocrine cells in the islets of Langerhans that respond to increases in blood glucose by secreting insulin and their dysfunction and death drives the development of diabetes. Beta cell senescence involving a DNA damage response (DDR) was recently shown to contribute to the pathogenesis of Type 1 Diabetes (T1D), however, a basic mechanistic understanding of how senescence develops in beta cells is lacking. Here, we investigated senescent phenotypes arising in the mouse beta cell line NIT1 derived from the T1D susceptible nonobese diabetic (NOD) mouse strain and the transcriptome response in human islets after induction of DNA damage. Sub-lethal DNA damage in NIT1 cells led to several classical hallmarks of senescence including the DDR, growth arrest, enlarged flattened morphology and a senescence-associated secretory phenotype (SASP) resembling what occurs during T1D. RNA-seq analysis on human islets with DNA double-strand break damage

revealed a coordinated p53-p21 transcriptional response and upregulation of genes involved in prosurvival signaling and SASP. Taken together, these findings suggest that some of the phenotypes of mouse and human beta cell senescence during T1D can be induced by DNA damage in NIT1 cells and human islets in culture.

Keywords: Pancreatic beta cells; Senescence; DNA damage response; Type 1 Diabetes

1. Introduction

Pancreatic beta cells reside as a terminally differentiated cell type in the islets of Langerhans and together with other islet cells comprise the endocrine compartment of the pancreas [1]. Beta cells play the unique role of responding to elevated blood glucose by secreting insulin, the essential hormone for glucose uptake and metabolism by peripheral tissues. The progressive death and dysfunction of beta cells disrupts islet function and is a driving factor in the pathogenesis of diabetes [2].

Cellular senescence is a complex and dynamic program of irreversible cell cycle arrest, typically initiated as a consequence of aging, oncogene activation, or a variety of stressors, and has many different biological purposes including tumor suppression, wound healing, tissue regeneration and embryonic patterning [3,4]. Senescence resulting from unrepairable cell stress or damage is usually activated via a combination of the $p16^{Ink4a}$/Rb and p53-p21 pathways, leading to permanent growth arrest and

hallmark phenotypes such as an enlarged cell morphology, elevated senescence-associated βgal activity (SA-βgal), persistent DNA damage response (DDR), apoptosis resistance and the senescence-associated secretory phenotype (SASP) [5]. Senescence progression and phenotypes are variable between cells and are generally cell type- and stress/trigger-dependent [6,7] and although well studied in vitro, are poorly understood in vivo, as there is no one marker that can accurately define senescence [8]. However, senescence culture models have been foundational in defining and characterizing critical molecular mechanisms and phenotypes that have been observed in vivo.

Recent work has demonstrated that a subpopulation of beta cells undergo senescence during the pathogenesis of Type 1 Diabetes [9], the form of the disease caused by selective autoimmune beta cell destruction [10]. While healthy beta cells are progressively destroyed by autoimmunity in T1D, senescent beta cells progressively accumulate in human T1D donors and in the preclinical nonobese diabetic (NOD) mouse model for T1D [9]. Senescent beta cells in NOD mice are characterized by upregulation of p21 and $p16^{Ink4a}$, DDR activation, a Bcl-2-mediated prosurvival phenotype, elevated SA-βgal activity and a SASP involving IL-6, Igfbp3, Serpine1, Mmp2, and Flnb [9,11]. The presence of DDR, Bcl-2 upregulation and SASP generally differentiates stress-induced senescence in beta cells from natural beta cell aging [12,13]. Notably, in NOD mice, elimination of senescent beta cells with Bcl-2 family inhibitors, or suppression of SASP, halts disease progression and ameliorates beta cell

dysfunction [9,14]. Therefore, senescence is a potential therapeutic target for T1D prevention.

Despite these advances, basic mechanistic questions around beta cell senescence in T1D remain. In particular, the specific triggers of senescence are not known and there is currently no mouse cell culture model to study the phenomenon. Different inbred mouse strains are used to model diabetes, each with different genetic background polymorphisms that could influence the development of specific senescence phenotypes. For instance, the NOD mouse strain commonly used as a model of T1D harbors two polymorphisms in the non-homologous end joining repair factor Xrcc4, lowering the efficiency of double-strand break repair in this strain as compared with C57BL strains [15]. Addressing fundamental mechanistic questions around beta cell senescence in T1D would greatly benefit from a culture model with the relevant genetic background.

As with NOD mice, a subset of beta cells in human T1D donors show DNA double-strand break damage and activation of the p53-p21 senescence pathway [9,11]. We previously showed that cultured primary adult human islets transcriptionally upregulate p21 (*CDKN1A)* gene expression and develop a SASP following induction of DNA double-strand breaks with the chemotherapeutic agent bleomycin [9,14]. These findings suggest that beta cell senescence in T1D may involve DNA double-strand break damage, but a comprehensive analysis of the outcomes of DDR induction in islets has

not been performed. Here, we investigated sub-lethal DNA double-strand break damage as a trigger for senescent phenotypes in the NIT1 cell line derived from the NOD mouse strain and its effects on the transcriptome of human islets. Our results suggest that chemically triggered DNA double-strand break damage in NIT1 cells and adult human islets accurately models some of the phenotypes involved in beta cell senescence during T1D and will be useful tools for understanding fundamental mechanisms.

2. Materials and Methods.

2.1 Mouse cell line culture and drug treatments.

Mouse insulinoma cell lines MIN6 (RRID:CVCL_0431, sex of cell line is unknown) derived from 13 week C57BL6 mice (gift from A. Bhushan, UCSF) and NIT1 (RRID: CVCL_3561), derived from 10 week female NOD/LtJ mice (purchased from ATCC) have been previously described[16,17]. Both cell lines were cultured in DMEM high glucose with 2 mM L-glutamine (ThermoFisher) containing 10% FBS (Millipore-Sigma), 20 mM HEPES, 1 mM sodium pyruvate (Gibco), 1X antibiotic-antimycotic (Gibco) and 50 µM 2-mercaptoethanol at 37°C and 5% CO_2. Cell lines were confirmed mycoplasma-free using the PlasmoTest mycoplasma kit (Invivogen). Cell lines were passaged after 4-6 days and MIN6 were detached with 0.25% trypsin-EDTA (Gibco) and seeded at 7.5-1x10^6 cells per 75 cm^2 flask, whereas NIT1 were detached with 0.05% trypsin-EDTA and seeded at 2-2.5x10^6 cells per flask. Cells were used between passages 4 and 25 for all experiments. For senescence induction, we modified a previous method that was used to trigger therapy-induced senescence in mouse melanoma cell line B16-F10[18]. MIN6 cells were seeded at a density of 0.7-0.85 x 10^5 cells/cm^2 in 12 or 6-well plates.

Twenty-four hours later, normal growth media was replaced with media containing 2 µM etoposide (Millipore-Sigma) or vehicle (0.01% DMSO) for 2-4 days, followed by removal of drug by replacing wells with fresh media. Similarly, NIT1 cells were seeded at a density of 0.85-1.15 x 10^5 cells/cm^2 and 24 h later cultured in 0.5 or 0.25 µM etoposide or vehicle (0.0025 or 0.00125% DMSO) for 3 or 4 days before drug removal as with MIN6 cells. After drug removal, the media was replaced with fresh media every other day. Vehicle-treated cells often reached confluence before drug washout and required passaging prior to drug washout, so cells were passaged into the same concentration of DMSO-containing media and media was replaced at the same time as the etoposide-treated cells. Cell counting and viability assays were performed with trypan blue staining on an automated cell counter (Bio-Rad TC-20). Cells were cultured for indicated times after drug treatment washout and harvested as indicated for various assays.

2.2 Human islet culture.

Human islets were procured through the Integrated Islet Distribution Program (IIDP) and the experiment was carried out at UCSF. Islets used for RNA-seq were isolated from a healthy nondiabetic female donor of Hispanic ethnicity, age 44 years with BMI of 24 and cause of death due to anoxia (RRID:SAMN13186657). Upon receipt islets were rested in culture for 24 h in RPMI-1640 media containing 10% FBS, 2 mM L-glutamine, 5.5 mM glucose and 1X antibiotic-antimycotic, as previously[9,14]. To induce DNA double-strand breaks and senescence, islets were cultured in media containing 50 µM bleomycin (Medchem express) or vehicle (0.2% DMSO) controls for 48 h, followed by removal and culture in drug-free media for 4 days, as previously[9]. Islets were then harvested for RNA extraction.

2.3 Western blot analysis.

Whole cell extracts were prepared with a commercial kit (RIPA cell protein extraction, ThermoFisher) in the presence of protease and phosphatase inhibitor cocktail (ThermoFisher) and protein was quantified with the BCA assay (ThermoFisher). Testis tissue from C57BL6/J 3 month old males was a gift from Dr. C. Doucette. Approximately 3-10µg of total protein from testis, MIN6 or NIT1 cells treated as indicated (equal amounts per sample) were electrophoresed on precast 4-12% gradient gels and electroblotted onto nitrocellulose membranes with the Bolt-iBlot2 system (ThermoFisher). Membranes were blocked in 5% non-fat milk in Tris buffered saline with 0.1% Tween-20 (TBST) for 1 h at room temperature. Primary antibodies used for westerns and dilutions used are indicated in **Supplementary Table 3**. Primary antibodies were incubated on membranes in TBST overnight at 4°C, washed three times for 5 minutes in TBST and detected with HRP-conjugated secondaries (Jackson Immunoresearch, diluted 1:50,000-1:100,000) after incubation for 1 h at room temperature in 5% non-fat milk in TBST. Membranes were washed three times for 5 minutes in TBST and were then incubated with SuperSignal West Pico Plus ECL (Thermo Fisher). Membranes were developed after exposure to X-ray film (Fuji Medical) and two or three exposures were collected to ensure signals were not saturated. Densitometry was performed using ImageJ to quantify band intensities relative to Beta actin. Original uncropped and annotated films are shown in **Supplementary Figure 6**.

2.4 SA-βgal activity assay.

SA-βgal activity in MIN6 and NIT1 cells was detected using a commercial kit (Cell Signaling Technology) according to the product instructions. Cells were subsequently washed in PBS and imaged on an EVOS color brightfield imager.

2.5 EdU labeling assay.

EdU incorporation was measured as an assay for DNA synthesis using a commercial kit (Abcam) according to the product instructions modified for adherent cells. Briefly, MIN6 or NIT1 cells were induced to senescence as indicated above and on the day of drug removal (72 h post-treatment) cells were incubated with media containing 5 µM EdU for 3 h at 37°C and 5% CO_2. Cells were subsequently washed with d-PBS, trypsinized, counted and resuspended at 1-5 x 10^6 cells/ml in d-PBS. The zombie NIR fixable viability kit (BioLegend) was used according to the manufacturer's instructions prior to fixation in 4% formaldehyde. After fixation, cell pellets were washed twice using cell staining buffer (BioLegend), permeabilized and treated with EdU detection solution. After two more washes, cells were filtered through a 70um strainer (ThermoFisher Scientific) into 5mL flow tubes (ThermoFisher Scientific). Flow cytometry was performed on an Attune acoustic focusing cytometer with a gating strategy as follows: FSC-A/SSC-A (cells), FSC-A/FSC-W (single cells), Zombie Near IR-negative (RL3, live cells) and EdU-positive (RL1). Approximately 4-10,000 live cells were scored per sample.

2.6 Luminex assays.

Conditioned media (CM) was collected by culturing cells in growth media lacking FBS overnight (18 h). CM was collected, clarified by centrifugation (3000g for 5 minutes at room temperature) and stored at 4°C for up to 1 month. Luminex assays were carried out on CM from cells treated as indicated using a custom magnetic bead kit that included Ccl4 and Ccl11 or IL-6, Serpine1 and Igfbp3 (R&D systems). 50 µl of CM was assayed on a Bio-Plex 200 luminex platform (Bio-Rad) as previously[9,14] and secreted amounts in 1-2 ml of CM were normalized to viable cell counts to calculate amount secreted per 100,000 cells.

2.7 EV secretion assays.

Control or etoposide treated Min6 and NIT1 cells were washed in d-PBS and cultured in growth media containing 10% bovine exosome-depleted FBS (Systems Bioscience International) on day 7 post-drug removal for 24 h and the conditioned media was collected and clarified by centrifugation at 3000g for 5 minutes. Total EVs were precipitated from CM using a polymer-based precipitation kit (Exo-Quick, Systems Bioscience) and resuspended in 150-200 µl of d-PBS. EV sample size distributions and concentrations were determined by nanotracking analysis (NTA) on a NanoSight NS300 (Malvern Instruments) after diluting 1:50:100 in d-PBS and using the following script: Set Viscosity = water, Syringe Load = 1000, Delay = 20, Syringe load = 40, Delay = 120, Repeat Start, Capture = 30, Delay =1, Repeat = 2, Syringe stop, Process single setting, and export results. Three technical replicates of particle counts and size distributions were determined from each sample. To calculate average EV secretion per cell, EV numbers/ml from the nanotracking analysis were multiplied by the starting CM

volume and were normalized to viable cell counts in each sample. NTA was carried out at the UCSF Parnassus Flow Core RRID:SCR_018206.

2.8 RNA extraction and quantitative RT-PCR.

Total RNA was extracted from MIN6, NIT1 or human islets using a commercial column-based purification with DNAse I treatment (Direct-Zol RNA MicroPrep with Trizol Reagent, Zymo Research). RNA was quantified by Nanodrop spectrophotometer (ThermoFisher Scientific). Approximately 300 ng of total RNA was used for cDNA synthesis with random primers (LunaScript SuperMix Kit, New England Biolabs). qPCR was carried out on a Bio-Rad CFX96 using Luna Universal qPCR Master Mix (New England BioLabs). Primers used for qPCR were previously validated from other studies and are indicated in **Supplementary Table 3**.

2.9 RNA-seq on human islets.

Approximately 1 µg of total RNA from bleomycin and vehicle-treated islets (n = 3 biological replicates per group) was submitted for paired-end RNA sequencing on Illumina Nova-Seq 6000 platform by a commercial service provider, LC Sciences. Total RNA was quality checked and ribosomal RNA depleted. Libraries were prepared with Illumina TruSeq-stranded total RNA sample protocol and quality checked by Agilent BioAnalyzer 2100 High Sensitivity DNA Chip. Cutadapt[19] and perl scripts were used to filter adapter contamination and undetermined bases. Sequences were quality checked with FastQC (https://www.bioinformatics.babraham.ac.uk/projects/fastqc)and mapped to the human genome (version 96) using Bowtie2 [20] and HISAT2 [21]. Mapped reads were assembled for each sample with StringTie[22] . A comprehensive

transcriptome was prepared using perl scripts and gffcompare (https://github.com/gpertea/gffcompare/). StringTie and edgeR[23] were used to estimate transcript expression levels. LncRNAs were identified based on filtering transcripts overlapping with known mRNAs, known lncRNAs and transcripts <200 bps. CPC[24] and CNCI[25] were used to predict transcripts coding potential. Transcripts with CPC score <-1 and CNCI score <0 were removed. Remaining transcripts were considered lncRNAs. StringTie was used to perform differential expression level analysis for mRNAs and lncRNAs by calculating FPKM (total exon fragments/mapped reads(millions) x exon length (kb)). A complete list of differentially and all expressed genes is shown in Supplementary Table 1. A complete list of differentially expressed lncRNAs and novel lncRNAs is found in Supplementary Table 2. Differentially expressed mRNAs and lncRNAs were selected with log2 fold-change >1 or <-1 between vehicle control and bleomycin treatment and parametric F-test comparing linear nested models ($p < 0.05$) by edgeR. GO and KEGG analysis was performed using by hypergeometric distribution fitting ($p < 0.05$) from gene ontology terms (http://www.geneontology.org) and KEGG pathways (http://www.kegg.jp).

2.10 Statistical analysis.

All statistical analyses were performed using GraphPad Prism version 9 with a minimum of n = 3 biological replicates per sample group. Statistical comparisons were performed with two-tailed unpaired T-test and were considered significant at $p < 0.05$.

3. Results

3.1 Sub-lethal etoposide treatment leads to senescent phenotypes in NIT1 cells

To develop a mouse beta cell culture model for senescence in T1D, we investigated senescent phenotypes in the NIT1 cell line, derived from a beta cell tumor in the T1D susceptible NOD/LtJ mouse strain [17] in response to DNA double-strand break damage. For comparison, we also examined the MIN6 beta cell line derived from the non-T1D susceptible C57BL6 strain [16], which was shown to develop senescent phenotypes in response to DNA damage with bleomycin [26]. Both lines have been immortalized via the expression of a rat insulin promoter driving the Simian virus 40 large T antigen (SV40 TAg). We induced DNA double-strand breaks using the topoisomerase II poison etoposide [27], as this drug has been used in the clinic to treat insulinomas [28] and hence it may be more effective in triggering therapy-induced senescence [29] as opposed to bleomycin. Of the two type II topoisomerase family members, we found that TopoIIα was expressed in both MIN6 cells and NIT1 cells, while TopoIIβ was expressed only in MIN6 (**Supplementary Figure 1A**) confirming that these cells express the target of this drug.

MIN6 or NIT1 cells were cultured in etoposide for 3 days, followed by drug removal to assay early senescent phenotypes or culturing the cells in drug-free media for an additional 5-14 days to assay late senescent phenotypes (**Figure 1A**). We titrated the doses of etoposide to maintain viability throughout the treatment and culture period.

While MIN6 cells tolerated 2 µM with >60% viability for up to 14 days post-drug removal, NIT1 could only survive in up to 0.5 µM for 7-9 days post-drug removal (**Figure 1B**) and similar results were obtained using 0.25 µM etoposide. Viability for both cell lines was maintained at ~80-90% during 72 h of drug treatment (**Figure 1B**) and cell counts only modestly decreased from the starting number seeded (**Supplementary Figure 1B**), suggesting that while some cell death was occurring, there was also a proliferation arrest during drug treatment.

Primary beta cells with DNA damage activate a canonical DDR involving the ATM-p53-21 pathway and phosphorylated KAP1^{Ser824} and phosphorylated Histone H2A.X^{Ser139} (gamma-H2A.X) [9,11,30,31]. Therefore, we next characterized DDR activation in NIT1 cells 24 h after etoposide treatment (**Figure 1C**). MIN6 cells exhibited a coordinated DDR with significant increases in phosphorylated ATM^{Ser1981}, p53, gamma-H2A.X, phosphorylated KAP1^{Ser824} and p21 (**Figure 1C**). In contrast, while NIT1 cells had increased activated ATM, phosphorylated KAP1 and induction of p21, there was no increase in p53 or gamma-H2A.X (**Figure 1C**). Activated p53 (phospho-p53^{Ser15}) was also detected in both undamaged and etoposide-treated MIN6 and NIT1 cells, but was not significantly increased relative to total p53 levels (**Supplementary Figure 2**). Total p53 and gamma-H2A.X were already abundant in undamaged NIT1 and MIN6 cells (**Figure 1C)**. Etoposide treatment also reduced the percent of MIN6 and NIT1 cells replicating DNA as indicated by a lower proportion of cells labeled with EdU at 72 h post-drug treatment (**Figure 1D**) consistent with a growth arrest. Similarly, etoposide treated MIN6 cells developed an enlarged flattened morphology with strong SA-βgal

activity by 5 days after drug removal, however, while NIT1 cells showed enlarged flattened morphology, they did not stain positive for SA-βgal activity at the same time point (**Figure 1E**). Taken together, these data show that NIT1 cells are more sensitive to DNA damage than MIN6 and that sub-lethal DNA double-strand break damage in these cells triggers DDR activation, growth arrest and senescence-related phenotypic changes, similar to MIN6.

3.2 Cdkn1a but not Cdkn2a is upregulated in growth arrested NIT1 cells

We next assessed whether CDK inhibitors p21 and/or p16^{Ink4a} were upregulated at later stages after drug removal in NIT1 cells (**Figure 2**). Notably, at the 72 h post-treatment timepoint, *Cdkn1a* but not *Cdkn2a* was upregulated in MIN6 cells and this persisted into late stage senescence at 14 days post-drug removal (**Figure 2A**), consistent with previous results [26]. Similarly, NIT1 cells also upregulated *Cdkn1a* expression at 72 h post-treatment and 7 days post-drug removal and also showed no upregulation of *Cdkn2a* (**Figure 2B**). Consistent with the early DDR-mediated induction of p21 (**Figure 1C**), elevated *Cdkn1a* expression was also reflected at the protein level 72 h post-treatment and 7 or 14 days post-drug removal in both lines, whereas again p16^{Ink4a} was not detected (**Figure 2B**). We also assessed the expression of Bcl-2, which is selectively upregulated during beta cell senescence in T1D and confers a prosurvival phenotype in senescent beta cells [9]. Notably, Bcl-2 was not detected in control or etoposide treated MIN6 cells or NIT1 cells (**Supplementary Figure 3**). Taken together these data suggest that senescent growth arrest in NIT1 involves p21 but not p16^{Ink4a} and does not involve Bcl-2 upregulation.

3.3 NIT1 cells develop a SASP

SASPs are cell-type and stressor-dependent, dynamic programs of secreted cytokines, chemokines, matrix proteases, shed receptors, growth factors, microRNAs and extracellular vesicles (EVs) that are immunogenic and have paracrine effects within the tissue microenvironment [32–34]. In senescent beta cells during pathogenesis of T1D in NOD mice, SASP comprises a wide variety factors such as interleukins (IL-6), chemokines (Cxcl10), growth factors (Igfbp3), and matrix metalloproteases and protease inhibitors (Mmp2, Serpine1) [9,14]. In contrast, EV secretion during beta cell senescence has not been explored. To determine whether etoposide-induced senescence in NIT1 cells involved SASP resembling primary beta cells in T1D, we assayed a panel of SASP factors found in T1D by a combination of western blot and luminex secretion assays and characterized EV secretion (**Figure 3**). Western blot of proenzyme and cleaved active Mmp2 isoforms revealed that etoposide treatment led to increased pro-Mmp2 levels in both MIN6 and NIT1 cells (**Figure 3A and 3B**). Luminex assays for SASP factors IL-6, Serpine1 and Igfbp3 [9] on conditioned media showed dramatically increased secretion of Serpine1 and Igfbp3, but not IL-6 from senescent NIT1 cells as compared with controls whereas none of these factors were secreted by senescent MIN6 cells (**Figure 3C and 3D**). In contrast, senescent MIN6 cells secreted Ccl11 and Ccl4 (**Supplementary Figure 4A**) consistent with previous reports [26,35] . Given that EV secretion is increased in senescent cells with DNA damage [36] we also assayed for total EV secretion from senescent NIT1 cells. Precipitation of EVs from undamaged control MIN6 and NIT1 cells revealed particles in the size range of 30-400

nm in diameter by nanotracking analysis, consistent with the sizes of both exosomes and microvesicles [37] and an average of 300-500 EVs secreted per cell in 24 h of culture (**Supplementary Figure 4B**). Senescent MIN6 and NIT1 cells showed a dramatic (>10-fold) increase in average EV secretion per cell compared with controls, reaching around 5,000-20,000 EVs per cell in 24 h of culture, in a temporal and drug dose dependent manner (**Figure 3E and 3F**). These data demonstrate that senescent NIT1 cells develop a SASP involving both soluble factors and increased EV secretion, and the SASP in NIT1 cells differs from MIN6.

3.4 Transcriptome analysis of DDR and early senescence in human islets reveals activation of the p53-p21 pathway

To further characterize our previously established human islet senescence model [9,14] and provide an unbiased analysis of the transcriptional responses following DNA damage, we performed RNA-seq on control or senescent human islets cultured ex vivo. Primary islets isolated from a healthy 44 year-old female donor were cultured with bleomycin to induce DNA double-strand breaks for 48 h and total islet RNA from the samples was extracted at 4 days post-drug removal for paired-end RNA-seq (**Figure 4A**). This timepoint is typically 1 day prior to the detection of SASP secretion in this model [9,14], and we reasoned that transcriptional changes in SASP genes would precede increased protein secretion, as SASP is controlled transcriptionally[6,14]. Differential expression analysis revealed 1690 genes significantly downregulated ≤0.5-fold and 201 genes significantly upregulated ≥2-fold ($p < 0.05$) (**Figure 4B**). A complete list of all genes with detected expression levels as fragments per kilobase per million reads (FPKM) are listed in Supplementary Table 1. Differentially expressed genes were

enriched for gene ontology (GO) terms including ‘cell division’ and ‘cell cycle’ (**Figure 4C**) and KEGG pathways ‘cell cycle’, ‘p53 signaling pathway’ and ‘PI3K-Akt signaling pathway’ (**Supplementary Figure 4A**). Genes involved in proliferation and cell cycle progression such as *MIK67, RRM2, TOP2A, CCNA2*, *CCNB2, MCM10, CDK1* were downregulated and p53 DDR pathway genes including *SPATA18, DDB2, GADD45A, GADD45G, ACER2, ZMAT3* [38] were upregulated (**Figure 4D**). In addition, p53 target gene *CDKN1A* was upregulated, but not other cyclin-dependent kinase inhibitor genes such as *CDKN2A*, *CDKN1B*, *CDKN1C, CDKN1D* or *CDKN2B* (**Figure 4D and Supplementary Table 1**). Gene expression changes associated with early senescence also occurred, including downregulation of *LMNB1* and *HMGB2* (**Figure 4D**) both of which occur during p53-mediated senescence induction in other cell types [39,40]. In addition to mRNAs, we also noted several small noncoding RNAs that were differentially expressed. These included *MIR34A*, a microRNA involved in senescence[41], along with *MIR3687-2* , *MIR3648-2, SNORA46 SNORA84, SNORD94* and *SNORD14B* which were all upregulated and *MIR22, MIR222, MIR143, MIR1-2*, *DNMOS3* were downregulated (**Supplementary Table 1**). We also found a group of previously annotated long noncoding RNAs (lncRNAs) that were differentially expressed and a group of predicted novel lncRNAs in bleomycin-treated islets (**Supplementary Table 2**). Notably among the lncRNAs, *DINOL* was found to be upregulated (**Supplementary Table 1**), consistent with its established role in amplifying p53-p21-mediated DDR signaling [42]. Together, these data validate that bleomycin treatment activates a p53-p21 DDR and early senescence transcriptional program in adult human islets.

3.5 DDR and senescence induction does not lead to loss of beta/islet cell gene programs or activation of UPR genes

To assess the effects of DDR activation and early senescence on beta cell/endocrine islet cell function we surveyed genes involved in hormone production and endocrine cell identity (**Figure 4E**). Genes encoding endocrine islet cell hormones and processing enzymes (*INS, GCG, SST, INSR, PCSK1, PCSK2, CPE*) and key beta/islet cell transcription factors (*PDX1, NKX6.1, MAFA, MAFB, NKX2.2, RFX6, ARX*) were surprisingly not changed (**Figure 4E**). The only exception was upregulation of *PCSK1N*, which encodes an endogenous inhibitor of the PCSK1 hormone processing enzyme that mediates proinsulin cleavage [43] (**Figure 4E**). Furthermore, genes involved in endoplasmic reticulum (ER) stress and unfolded protein response (UPR) (*XBP1, DDIT3, EDEM1, ERN1, ATF4, ATF6, HSPA5, HSP90B1*), which are involved in beta cell adaptive and terminal UPR, were not significantly changed between control and bleomycin treatment (**Supplementary Figure 6**). Comparison of the list of differentially expressed genes in our dataset with recently generated human islet RNA-seq datasets during aging [44] and adult human islets treated with the cytokine IFNα [45] showed that there were only 74/385 (~19%) age-related genes in common and only 256/1894 (~13%) IFNα-regulated genes in common, respectively, (**Supplementary Figure 7A and 7B, Supplementary Table 1**). This suggested that the transcriptional response during islet DDR activation and senescence is generally different from natural aging and cytokine exposure.

3.6 Expression of BCL-2 family genes and SASP genes in islet DDR and senescence

To assess whether islet cells were undergoing senescence, we next looked at genes involved in critical senescence phenotypes, prosurvival signaling involving BCL-2 family

prosurvival genes and SASP. Among the prosurvival family members, *BCL2L1, MCL1* and *BCL2L2* were the only members expressed at appreciable levels, and of these only *BCL2L1* (encoding BCL-XL) was significantly upregulated (**Figure 4F**). Assessment of genes encoding canonical SASP factors such as *IL6, CXCL8, SERPINE1, IGFBP3, CXCL1, IGFBP4, MMP1, MMP2* revealed that the majority of them were either dramatically downregulated or unchanged in bleomycin treated islets relative to controls (**Figure 4G, Supplementary Table 1**). However, among the significantly upregulated genes, we noted several previously identified SASP genes encoding secreted factors and cell surface receptors, including *GDF15, CXCL5, CCL11, TNFRSFC10C, TNFRSF10A* and *SERPINA6* [7,26,32,46,47] (**Figure 4G**). We also noted upregulation of several TGFβ/NOTCH pathway genes, including *HES5, HES2*, and *DLK1* (**Supplementary Table 1**), which may contribute to the early TGFβ-driven SASP that occurs prior to the switch into the canonical proinflammatory SASP in late senescence [48]. Taken together, these results suggest that islet DDR activation leads to development of early senescence transcriptional changes, including activation of BCL-2 family prosurvival gene *BCL2L1* and a subset of early TGFβ-related SASP genes.

4. Discussion

Pancreatic beta cell senescence occurs as a stress response during progression and onset of T1D [9], but the triggers that lead to senescence are poorly understood. The use of cell culture models has been indispensable for the field of senescence and has formed the basis for understanding the mechanisms underpinning this complex process. As senescent beta cells in T1D show DDR activation [9,11], we carried out culture

assays and RNA-seq to determine the extent to which the induction of DNA damage in the NIT1 cell line derived from a T1D-susceptible mouse strain and adult human islets recapitulates features of beta cell senescence in T1D. We demonstrated that NIT1 responded to sub-lethal DNA double-strand break damage with etoposide by activating the DDR, growth arrest, developing an enlarged flattened morphology and a SASP resembling what is observed in T1D. There were differences in these phenotypes as compared with MIN6 cells, derived from a non-T1D susceptible mouse strain, pointing to the role of genetic background in modifying the outcomes of beta cell DDR. Consistent with previous findings revealing polymorphisms that reduce the efficiency of DNA repair in NOD/ShiLtJ as compared with C57BL10 embryonic fibroblasts [15], NIT1 cells were more sensitive to DNA double-strand break damage as compared with MIN6. In addition, although they were clearly growth arrested and developed an enlarged and flattened morphology, NIT1 cells did not develop high SA-βgal activity like MIN6 cells, and this also differs from beta cell senescence in human T1D donors [9]. Both cell lines upregulated *Cdkn1a* expression at the gene and protein levels but not *Cdkn2a*, suggesting that growth arrest relies on p21 rather than $p16^{Ink4a}$. Furthermore, Bcl-2 was not detected in NIT1 or MIN6 cells and consistent with a lack of prosurvival phenotype, these lines showed declining viability in culture at late stages. Interestingly, NIT1 cells developed a SASP involving factors found in T1D, whereas the SASP in MIN6 involved different factors. Altered EV secretion is a recently emerging, but unclear aspect of SASP [32] and has not been studied in senescent beta cells. Our results with NIT1 cells suggest that increased EV secretion may be a feature of beta cell senescence during T1D. Future studies will be required to investigate the cargo of senescent beta cell EVs.

Taken as a whole, these results suggest that specific aspects of mouse beta cell senescence in T1D, including DDR activation, growth arrest and SASP, but not SA-βgal activity or Bcl-2 prosurvival phenotype can be modeled using NIT1 cells treated with etoposide.

Human islets show substantial differences in architecture, metabolism, and proliferative capacity as compared with rodents [49], necessitating the study of beta cell senescence in human cell models. We previously established a primary human islet model for DDR and SASP using the DNA double-strand break agent bleomycin and found that it induces some of the same phenotypes observed during beta cell senescence in human T1D donors [9] but a systematic interrogation of this model was lacking. Using an unbiased analysis by RNA-seq, we found that DDR activation and senescence induction with bleomycin resulted in a coordinated p53-p21 transcriptional program, involving downregulation of many genes involved in proliferation and cell cycle progression and upregulation of p53-targeted genes. Although there were a small subset of genes in common with other human islet RNA-seq datasets representing natural aging [44] or cytokine exposure [45] the changes during islet DDR activation and senescence were largely distinct. Importantly, the changes in this model occur 4 days after drug removal (6 days post-treatment) and thus reflect a stable phenotypic change rather than an acute response. Notable among these changes was the robust upregulation of *CDKN1A* and no increases in *CDKN2A* expression, consistent with our earlier analysis by qRT-PCR in this model and protein-level changes in beta cells of T1D donors [9]. While *CDKN2A* gene expression was not induced in islets after DDR and early senescence,

p16^{INK4A} protein level is already very abundant in middle-aged adult donor pancreas and islets [9,50,51], thus the gene expression level is likely not an accurate reflection of the protein levels. Remarkably, there were no significant changes in islet cell hormone genes, lineage identity genes, or UPR genes at this timepoint after DDR activation and early senescence. While this suggests that DDR and early senescence do not significantly impact islet identity and UPR, it cannot be ruled out that the cells that had altered beta cell/islet cell identity, hormone, or UPR gene expression had already undergone apoptosis and thus were not present in the assay at this timepoint. Moreover, as many changes will occur at the protein level, further assays on islet identity proteins and UPR factors is needed.

In addition to a p53-p21 DDR transcriptional response in bleomycin-treated islets, we also found evidence for two other senescence phenotypes, BCL-2 family gene upregulation and an early SASP. We identified selective upregulation of BCL2 family member gene *BCL2L1* in bleomycin treated islets. The BCL-2 family of anti-apoptotic proteins confer a prosurvival phenotype on senescent cells and *BCL2L1* encodes BCL-XL, which is known to be upregulated at the mRNA and protein level in other cell types during senescence [52,53]. Thus, it will be interesting to investigate whether BCL-XL is upregulated during beta cell senescence in T1D donors and confers a prosurvival phenotype to senescent human beta cells. While many proinflammatory SASP genes were downregulated, a subset of TGFβ-related SASP genes encoding secreted factors and cell surface receptors were significantly upregulated. Notable among them was *GDF15*, recently identified as a beta cell SASP factor in mice in a T2D model [26].

Together, the BCL-2 family gene expression and SASP gene transcriptional changes are consistent with the induction of a bona fide DNA damage-induced senescence program as opposed to an apoptotic response.

While our RNA-seq dataset provides a novel resource to explore transcriptional programs of beta/islet cell senescence in humans during T1D, a major limitation of this model is that it is a mixed cell population, since islets are comprised of several endocrine and non-endocrine cell types. Thus, it cannot be determined which specific cell types are undergoing DDR and senescence in this system. Further studies will be necessary using cell sorting or single-cell transcriptomics to investigate the expression of specific DDR and senescence-associated genes in different islet cell types. In conclusion, our findings substantiate DNA double-strand break damage in mouse NIT1 cells and human islets as culture models for beta cell senescence occurring during T1D. Despite their limitations, these models will be useful for further dissecting the molecular mechanisms and functional consequences of senescence and its contributions to the pathogenesis of T1D.

Acknowledgements. The authors thank Dr. Anil Bhushan at University of California San Francisco (UCSF), who is supported by NIH R01DK121794 and R01DK118099 for providing resources for PJT to carry out the RNA-seq on human islets and the EV studies while a postdoctoral fellow in his lab.

Disclosure statement.

No potential conflict of interest was reported by the author(s).

Availability of Data and Materials.

The RNA-seq raw data and processed data files described in this study are publicly available on NCBI GEO Accession number GSE176324. Expression data tables are also available in Supplementary Information.

Funding

While at UCSF, PJT was supported in the lab of Dr. Anil Bhushan by a postdoctoral fellowship from the Larry L. Hillblom Foundation and a UCSF Program for Breakthrough Biomedical Research postdoctoral award. This study was supported in part by start-up funds awarded to PJT from the University of Manitoba and the Children's Hospital Research Institute of Manitoba.

Figure Legends.

Figure 1. Etoposide induces DDR, growth arrest and senescent morphology in MIN6 and NIT1 cells.

(A) MIN6 cells (derived from C57BL6 mouse beta cell tumor) or NIT1 cells (derived from NOD/LtJ mouse beta cell tumor) were seeded and treated with etoposide (2 µM for MIN6, 0.25-0.5 µM for NIT1) or vehicle control (DMSO) for 72 hrs. Drug was removed by changing cells into fresh media, and cells were cultured an additional 5-14 days before final harvests. Early senescence phenotypes were monitored at 24-72 hrs post-etoposide treatment and late phenotypes were assayed at 5-14 days post drug removal.

B) Cell viability was scored at 24 or 72 hrs after etoposide treatment and 7 or 14 days post-drug removal. Data are mean ± SD of n = 3-6 biological replicates.

C) Western blot analysis and relative quantifications of DDR activation markers in MIN6 and NIT1 cells at 24 h post etoposide or vehicle treatment. Data are mean ± SD of n = 3 biological replicates.

D) EdU labeling flow cytometry assay for DNA replication at 72 hrs post-etoposide or vehicle control treatment of MIN6 or NIT1 cells. 'Ctrl' indicates a no EdU negative control population of cells. Data are mean ± SD of n = 3 biological replicates.

E) Representative images of Xgal staining for SA-βgal activity in MIN6 and NIT1 cells at day 5 post-drug removal. Scale bar = 30 µm.

*$p < 0.05$, **$p < 0.005$, ***$p < 0.0005$, ****$p < 0.00005$, unpaired two-tailed T-tests.

Figure 2. Induction of *Cdkn1a* but not *Cdkn2a* at mRNA and protein level in etoposide treated MIN6 and NIT1 cells

A) qRT-PCR analysis of *Cdkn1a* and *Cdkn2a* expression normalized to *Gapdh* in MIN6 cells at 72 hrs post-etoposide or vehicle treatment or 14 days post-drug removal (as from Fig. 1). Data are mean ± SD of n = 3 biological replicates.

B) qRT-PCR analysis as in B) except on NIT1 cells at 72 hrs and 7 days post-drug removal.

C) Western blot of p21 and $p16^{Ink4a}$ on whole cell extracts from MIN6 cells treated with 2 µM etoposide or vehicle control 14 days post-drug removal, Actin was a loading control and whole cell extract from 3 month old C57BL6 mouse testes was a positive control for p21 and p16. P21 quantification relative to actin is mean ± SD of n = 3 biological replicates. Data are mean ± SD of n = 3 biological replicates.

D) Western blot of p21 on whole cell extracts from NIT1 cells treated with 0.25 µM etoposide or vehicle at 6 days post-drug removal. Data are mean ± SD of n = 3 biological replicates.

For all panels, *p < 0.05, **p< 0.005, ***p < 0.0005, ns = not significant, two-tailed T-tests.

Figure 3. NIT1 cells develop a SASP.

A) and B) Western blot analysis of Pro-Mmp2 (70 kDa) and cleaved/activated Mmp2 (62 kDa) on whole cell extracts from MIN6 or NIT1 cells treated with vehicle or etoposide as indicated. Quantification shows relative Pro-Mmp2 or Cleaved Mmp2 to Actin, mean ± SD of n = 3 biological replicates.

C) and D) Luminex assay of secreted SASP factors IL-6, Serpine1 and Igfbp3 in serum-free conditioned media from MIN6 or NIT1 cells treated as indicated at timepoints indicated. Data are mean ± SD from n = 3 biological replicates.

E) Nanotracking analysis size and concentration histogram of EVs isolated from vehicle control or etoposide treated MIN6 (2 µM) or NIT1 cells (0.5 µM) at day 8 post-drug removal. Mean indicates the average diameter of the particles for each sample from three technical replicate measurements.

F) Quantification of average EV secretion per cell from control and etoposide treated MIN6 or NIT1 cells at the timepoints indicated, or with the etoposide concentrations indicated. Data are mean ± SD of three technical replicate measurements per sample.

For all panels, *p< 0.05, **p<0.005, ***p<0.0005, ns = not significant, two-tailed T-tests

Figure 4. Transcriptome analysis of human islet DDR and early senescence reveals activation of the p53-p21 pathway.

A) Overview of human islet DDR and senescence model. Islets isolated from a 44 year-old female donor were rested overnight and then divided into a total of 6 wells and cultured in the presence of vehicle (DMSO) or 50 µM bleomycin for 48 h (n = 3 biological replicates per group). The islets were then transferred to fresh drug-free media and cultured an additional 4 days prior to harvesting on day 5 post-drug removal for RNA extraction and paired-end RNA-seq.

B) Volcano plot of differentially expressed genes ($p < 0.05$) indicating 1690 genes downregulated ≤0.5-fold and 201 genes upregulated ≥2-fold in bleomycin treated islets compared to controls.

C) Significant GO terms of differentially expressed genes.

D) Plot of normalized expression levels (FPKM) of selected significantly downregulated proliferation and cell cycle genes.

E) Plot of normalized expression levels of significantly upregulated p53-p21 DDR genes and two early senescence genes (*LMNB1* and *HMGB2*).

F) Plot of normalized expression levels of selected islet cell identity and hormone genes. None of these genes were differentially expressed except *PCSK1N* which was significantly upregulated in bleo versus control (*$p < 0.05$).

G) Plot of selected BCL-2 family anti-apoptotic genes. Only *BCL2L1* was significantly upregulated, (*$p < 0.05$).

H) Plot of selected downregulated proinflammatory SASP genes and upregulated early islet SASP genes, all with significantly different expression between vehicle and bleomycin-treated islets.

References

[1] G.M. Noguchi, M.O. Huising, Integrating the inputs that shape pancreatic islet hormone release, Nat. Metab. 1 (2019) 1189–1201. https://doi.org/10.1038/s42255-019-0148-2.

[2] D.L. Eizirik, L. Pasquali, M. Cnop, Pancreatic β-cells in type 1 and type 2 diabetes mellitus: different pathways to failure, Nat. Rev. Endocrinol. 16 (2020) 349–362. https://doi.org/10.1038/s41574-020-0355-7.

[3] S. He, N.E. Sharpless, Senescence in Health and Disease, Cell. 169 (2017) 1000–1011. https://doi.org/10.1016/j.cell.2017.05.015.

[4] N. Herranz, J. Gil, Mechanisms and functions of cellular senescence, J. Clin. Invest. 128 (2018) 1238–1246. https://doi.org/10.1172/JCI95148.

[5] B.G. Childs, M. Gluscevic, D.J. Baker, R.M. Laberge, D. Marquess, J. Dananberg, J.M. Van Deursen, Senescent cells: An emerging target for diseases of ageing, Nat. Rev. Drug Discov. 16 (2017) 718–735. https://doi.org/10.1038/nrd.2017.116.

[6] A. Hernandez-Segura, T. V. de Jong, S. Melov, V. Guryev, J. Campisi, M. Demaria, Unmasking Transcriptional Heterogeneity in Senescent Cells, Curr. Biol. 27 (2017) 2652-2660.e4. https://doi.org/10.1016/j.cub.2017.07.033.

[7] C.D. Wiley, J.M. Flynn, C. Morrissey, R. Lebofsky, J. Shuga, X. Dong, M.A. Unger, J. Vijg, S. Melov, J. Campisi, Analysis of individual cells identifies cell-to-cell variability following induction of cellular senescence, Aging Cell. 16 (2017) 1043–1050. https://doi.org/10.1111/acel.12632.

[8] N.E. Sharpless, C.J. Sherr, Forging a signature of in vivo senescence, Nat. Rev. Cancer. 15 (2015) 397–408. https://doi.org/10.1038/nrc3960.

[9] P.J. Thompson, A. Shah, V. Ntranos, F. Van Gool, M. Atkinson, A. Bhushan, Targeted Elimination of Senescent Beta Cells Prevents Type 1 Diabetes, Cell Metab. 29 (2019) 1045–60. https://doi.org/10.1016/j.cmet.2019.01.021.

[10] A. Katsarou, S. Gudbjornsdottir, A. Rawshani, D. Dabelea, E. Bonifacio, B.J. Anderson, L.M. Jacobsen, D.A. Schatz, A. Lernmark, Type 1 diabetes mellitus., Nat. Rev. Dis. Prim. 3 (2017) 17016. https://doi.org/10.1038/nrdp.2017.16.

[11] E. Horwitz, L. Krogvold, S. Zhitomirsky, A. Swisa, M. Fischman, T. Lax, T. Dahan, N. Hurvitz, N. Weinberg-Corem, A. Klochendler, A.C. Powers, M. Brissova, A. Jorns, S. Lenzen, B. Glaser, K. Dahl-Jorgensen, Y. Dor, Beta Cell DNA Damage Response Promotes Islet Inflammation in Type 1 Diabetes., Diabetes. (2018).

https://doi.org/10.2337/db17-1006.

[12] A. Helman, D. Avrahami, A. Klochendler, B. Glaser, K.H. Kaestner, I. Ben-Porath, Y. Dor, Effects of ageing and senescence on pancreatic β-cell function, Diabetes, Obes. Metab. 18 (2016) 58–62. https://doi.org/10.1111/dom.12719.

[13] G. Brawerman, P.J. Thompson, Beta cell therapies for preventing type 1 diabetes: From bench to bedside, Biomolecules. 10 (2020) 1–20. https://doi.org/10.3390/biom10121681.

[14] P.J. Thompson, A. Shah, H. Apostolopolou, A. Bhushan, BET proteins are required for transcriptional activation of the senescent islet cell secretome in type 1 diabetes, Int. J. Mol. Sci. 20 (2019) 1–13. https://doi.org/10.3390/ijms20194776.

[15] J. Dooley, L. Tian, S. Schonefeldt, V. Delghingaro-Augusto, J.E. Garcia-Perez, E. Pasciuto, D. Di Marino, E.J. Carr, N. Oskolkov, V. Lyssenko, D. Franckaert, V. Lagou, L. Overbergh, J. Vandenbussche, J. Allemeersch, G. Chabot-Roy, J.E. Dahlstrom, D.R. Laybutt, N. Petrovsky, L. Socha, K. Gevaert, A.M. Jetten, D. Lambrechts, M.A. Linterman, C.C. Goodnow, C.J. Nolan, S. Lesage, S.M. Schlenner, A. Liston, Genetic predisposition for beta cell fragility underlies type 1 and type 2 diabetes., Nat. Genet. 48 (2016) 519–527. https://doi.org/10.1038/ng.3531.

[16] J.I. Miyazaki, K. Araki, E. Yamato, H. Ikegami, T. Asano, Y. Shibasaki, Y. Oka, K.I. Yamamura, J.I. Miyazaki, Establishment of a pancreatic β cell line that retains glucose-inducible insulin secretion: Special reference to expression of glucose transporter isoforms, Endocrinology. 127 (1990) 126–132. https://doi.org/10.1210/endo-127-1-126.

[17] K. Hamaguchi, H.R. Gaskins, E.H. Leiter, NIT-1, a pancreatic β-cell line established from a transgenic NOD/Lt mouse, Diabetes. 40 (1991) 842–849. https://doi.org/10.2337/diab.40.7.842.

[18] A.C. Flor, D. Wolfgeher, D. Wu, S.J. Kron, A signature of enhanced lipid metabolism, lipid peroxidation and aldehyde stress in therapy-induced senescence, Cell Death Discov. 3 (2017) 1–12. https://doi.org/10.1038/cddiscovery.2017.75.

[19] M. Martin, Cutadapt removes adapter sequences from high-throughput sequencing reads, Embnet J. 17 (2011) 10–12.

[20] B. Langmead, S.L. Salzberg, Fast gapped-read alignment with Bowtie 2., Nat. Methods. 9 (2012) 357–359. https://doi.org/10.1038/nmeth.1923.

[21] D. Kim, B. Langmead, S.L. Salzberg, HISAT: a fast spliced aligner with low memory requirements., Nat. Methods. 12 (2015) 357–360. https://doi.org/10.1038/nmeth.3317.

[22] M. Pertea, G.M. Pertea, C.M. Antonescu, T.-C. Chang, J.T. Mendell, S.L. Salzberg, StringTie enables improved reconstruction of a transcriptome from RNA-seq reads., Nat. Biotechnol. 33 (2015) 290–295.

https://doi.org/10.1038/nbt.3122.

[23] M.D. Robinson, D.J. McCarthy, G.K. Smyth, edgeR: a Bioconductor package for differential expression analysis of digital gene expression data., Bioinformatics. 26 (2010) 139–140. https://doi.org/10.1093/bioinformatics/btp616.

[24] L. Kong, Y. Zhang, Z.-Q. Ye, X.-Q. Liu, S.-Q. Zhao, L. Wei, G. Gao, CPC: assess the protein-coding potential of transcripts using sequence features and support vector machine., Nucleic Acids Res. 35 (2007) W345-9. https://doi.org/10.1093/nar/gkm391.

[25] L. Sun, H. Luo, D. Bu, G. Zhao, K. Yu, C. Zhang, Y. Liu, R. Chen, Y. Zhao, Utilizing sequence intrinsic composition to classify protein-coding and long non-coding transcripts., Nucleic Acids Res. 41 (2013) e166. https://doi.org/10.1093/nar/gkt646.

[26] A. Midha, H. Pan, C. Abarca, J. Andle, P. Carapeto, S. Bonner-Weir, C. Aguayo-Mazzucato, Unique human and mouse β-cell senescence-associated secretory phenotype (SASP) reveal conserved signaling pathways and heterogeneous factors., Diabetes. (2021). https://doi.org/10.2337/db20-0553.

[27] S.J. Froelich-Ammon, N. Osheroff, Topoisomerase poisons: Harnessing the dark side of enzyme mechanism, J. Biol. Chem. 270 (1995) 21429–21432. https://doi.org/10.1074/jbc.270.37.21429.

[28] E. Brown, D. Watkin, J. Evans, V. Yip, D.J. Cuthbertson, Multidisciplinary management of refractory insulinomas, Clin. Endocrinol. (Oxf). 88 (2018) 615–624. https://doi.org/10.1111/cen.13528.

[29] P.G. Prasanna, D.E. Citrin, J. Hildesheim, M.M. Ahmed, S. Venkatachalam, G. Riscuta, D. Xi, G. Zheng, J. van Deursen, J. Goronzy, S.J. Kron, M.S. Anscher, N.E. Sharpless, J. Campisi, S.L. Brown, L.J. Niedernhofer, A. O'Loghlen, A.G. Georgakilas, F. Paris, D. Gius, D.A. Gewirtz, C.A. Schmitt, M.E. Abazeed, J.L. Kirkland, A. Richmond, P.B. Romesser, S.W. Lowe, J. Gil, M.S. Mendonca, S. Burma, D. Zhou, C.N. Coleman, Therapy-Induced Senescence: Opportunities to Improve Anti-Cancer Therapy., J. Natl. Cancer Inst. (2021). https://doi.org/10.1093/jnci/djab064.

[30] O. Tavana, N. Puebla-osorio, M. Sang, C. Zhu, Nonhomologous End-Joining Deficiency Leads to a Severe Diabetic Phenotype in Mice, Diabetes. 59 (2010). https://doi.org/10.2337/db09-0792.O.T.

[31] V. Chesnokova, C. Wong, S. Zonis, A. Gruszka, K. Wawrowsky, Diminished pancreatic beta-cell mass in securin-null mice is caused by beta-cell apoptosis and senescence., Endocrinology. 150 (2009) 2603–2610. https://doi.org/10.1210/en.2008-0972.

[32] N. Basisty, A. Kale, O.H. Jeon, C. Kuehnemann, T. Payne, C. Rao, A. Holtz, S. Shah, V. Sharma, L. Ferrucci, J. Campisi, B. Schilling, A Proteomic Atlas of Senescence-Associated Secretomes for Aging Biomarker Development, BioRxiv. (2019) 1–26. https://doi.org/10.1101/604306.

[33] M. Paez-Ribes, E. González-Gualda, G.J. Doherty, D. Muñoz-Espín, Targeting senescent cells in translational medicine, EMBO Mol. Med. 11 (2019) 1–19. https://doi.org/10.15252/emmm.201810234.

[34] L.G.P.L. Prata, I.G. Ovsyannikova, T. Tchkonia, J.L. Kirkland, Senescent cell clearance by the immune system: Emerging therapeutic opportunities, Semin. Immunol. 40 (2018) 101275. https://doi.org/10.1016/j.smim.2019.04.003.

[35] C. Aguayo-Mazzucato, J. Andle, T.B. Lee, A. Midha, L. Talemal, V. Chipashvili, J. Hollister-Lock, J. van Deursen, G. Weir, S. Bonner-Weir, Acceleration of β Cell Aging Determines Diabetes and Senolysis Improves Disease Outcomes, Cell Metab. 30 (2019) 129-142.e4. https://doi.org/10.1016/j.cmet.2019.05.006.

[36] A. Takahashi, R. Okada, K. Nagao, Y. Kawamata, A. Hanyu, S. Yoshimoto, M. Takasugi, S. Watanabe, M.T. Kanemaki, C. Obuse, E. Hara, Exosomes maintain cellular homeostasis by excreting harmful DNA from cells, Nat. Commun. 8 (2017) 1–14. https://doi.org/10.1038/ncomms15287.

[37] M. Colombo, G. Raposo, C. Théry, Biogenesis, Secretion, and Intercellular Interactions of Exosomes and Other Extracellular Vesicles, Annu. Rev. Cell Dev. Biol. 30 (2014) 255–289. https://doi.org/10.1146/annurev-cellbio-101512-122326.

[38] M. Fischer, Census and evaluation of p53 target genes, Oncogene. 36 (2017) 3943–3956. https://doi.org/10.1038/onc.2016.502.

[39] A. Freund, R.-M. Laberge, M. Demaria, J. Campisi, Lamin B1 loss is a senescence-associated biomarker., Mol. Biol. Cell. 23 (2012) 2066–75. https://doi.org/10.1091/mbc.E11-10-0884.

[40] K.M. Aird, O. Iwasaki, A. V. Kossenkov, H. Tanizawa, N. Fatkhutdinov, B.G. Bitler, L. Le, G. Alicea, T.L. Yang, F.B. Johnson, K.I. Noma, R. Zhang, HMGB2 orchestrates the chromatin landscape of senescence-associated secretory phenotype gene loci, J. Cell Biol. 215 (2016) 325–334. https://doi.org/10.1083/jcb.201608026.

[41] F.J. Liu, T. Wen, L. Liu, MicroRNAs as a novel cellular senescence regulator, Ageing Res. Rev. 11 (2012) 41–50. https://doi.org/10.1016/j.arr.2011.06.001.

[42] A.M. Schmitt, J.T. Garcia, T. Hung, R.A. Flynn, Y. Shen, K. Qu, A.Y. Payumo, A. Peres-Da-Silva, D.K. Broz, R. Baum, S. Guo, J.K. Chen, L.D. Attardi, H.Y. Chang, An inducible long noncoding RNA amplifies DNA damage signaling, Nat. Genet. 48 (2016) 1370–1376. https://doi.org/10.1038/ng.3673.

[43] Y.C. Chen, A.J. Taylor, C.B. Verchere, Islet prohormone processing in health and disease, Diabetes, Obes. Metab. 20 (2018) 64–76. https://doi.org/10.1111/dom.13401.

[44] P. Seiron, A. Stenwall, A. Hedin, L. Granlund, J.L.S. Esguerra, P. Volkov, E. Renström, O. Korsgren, M. Lundberg, O. Skog, Transcriptional analysis of islets of Langerhans from organ donors of different ages, PLoS One. 16 (2021) 1–13. https://doi.org/10.1371/journal.pone.0247888.

[45] M.L. Colli, M. Ramos-Rodríguez, E.S. Nakayasu, M.I. Alvelos, M. Lopes, J.L.E. Hill, J.V. Turatsinze, A. Coomans de Brachène, M.A. Russell, H. Raurell-Vila, A. Castela, J. Juan-Mateu, B.J.M. Webb-Robertson, L. Krogvold, K. Dahl-Jorgensen, L. Marselli, P. Marchetti, S.J. Richardson, N.G. Morgan, T.O. Metz, L. Pasquali, D.L. Eizirik, An integrated multi-omics approach identifies the landscape of interferon-α-mediated responses of human pancreatic beta cells, Nat. Commun. 11 (2020). https://doi.org/10.1038/s41467-020-16327-0.

[46] Z. Novakova, S. Hubackova, M. Kosar, L. Janderova-Rossmeislova, J. Dobrovolna, P. Vasicova, M. Vancurova, Z. Horejsi, P. Hozak, J. Bartek, Z. Hodny, Cytokine expression and signaling in drug-induced cellular senescence, Oncogene. 29 (2010) 273–284. https://doi.org/10.1038/onc.2009.318.

[47] K.M. Irvine, R. Skoien, N.J. Bokil, M. Melino, G.P. Thomas, D. Loo, B. Gabrielli, M.M. Hill, M.J. Sweet, A.D. Clouston, E.E. Powell, Senescent human hepatocytes express a unique secretory phenotype and promote macrophage migration, World J. Gastroenterol. 20 (2014) 17851–17862. https://doi.org/10.3748/wjg.v20.i47.17851.

[48] M. Hoare, Y. Ito, T.-W. Kang, M.P. Weekes, N.J. Matheson, D.A. Patten, S. Shetty, A.J. Parry, S. Menon, R. Salama, R. Antrobus, K. Tomimatsu, W. Howat, P.J. Lehner, L. Zender, M. Narita, NOTCH1 mediates a switch between two distinct secretomes during senescence, Nat. Cell Biol. 18 (2016) 979–992. https://doi.org/10.1038/ncb3397.

[49] D.J. Steiner, A. Kim, K. Miller, M. Hara, Pancreatic islet plasticity: Interspecies comparison of islet architecture and composition, Islets. 2 (2010). https://doi.org/10.4161/isl.2.3.11815.

[50] A. Helman, A. Klochendler, N. Azazmeh, Y. Gabai, E. Horwitz, S. Anzi, A. Swisa, R. Condiotti, R.Z. Granit, Y. Nevo, Y. Fixler, D. Shreibman, A. Zamir, S. Tornovsky-Babeay, C. Dai, B. Glaser, A.C. Powers, A.M.J. Shapiro, M.A. Magnuson, Y. Dor, I. Ben-Porath, p16(Ink4a)-induced senescence of pancreatic beta cells enhances insulin secretion., Nat. Med. 22 (2016) 412–20. https://doi.org/10.1038/nm.4054.

[51] C.U. Köhler, M. Olewinski, A. Tannapfel, W.E. Schmidt, H. Fritsch, J.J. Meier, Cell cycle control of β-cell replication in the prenatal and postnatal human pancreas, Am. J. Physiol. - Endocrinol. Metab. 300 (2011). https://doi.org/10.1152/ajpendo.00496.2010.

[52] Y. Zhu, T. Tchkonia, T. Pirtskhalava, A.C. Gower, H. Ding, N. Giorgadze, A.K. Palmer, Y. Ikeno, G.B. Hubbard, M. Lenburg, S.P. O'Hara, N.F. Larusso, J.D. Miller, C.M. Roos, G.C. Verzosa, N.K. Lebrasseur, J.D. Wren, J.N. Farr, S. Khosla, M.B. Stout, S.J. Mcgowan, H. Fuhrmann-Stroissnigg, A.U. Gurkar, J. Zhao, D. Colangelo, A. Dorronsoro, Y.Y. Ling, A.S. Barghouthy, D.C. Navarro, T. Sano, P.D. Robbins, L.J. Niedernhofer, J.L. Kirkland, The Achilles' heel of senescent cells: From transcriptome to senolytic drugs, Aging Cell. (2015) 644–658. https://doi.org/10.1111/acel.12344.

[53] R. Yosef, N. Pilpel, R. Tokarsky-Amiel, A. Biran, Y. Ovadya, S. Cohen, E. Vadai, L. Dassa, E. Shahar, R. Condiotti, I. Ben-Porath, V. Krizhanovsky, Directed elimination of senescent cells by inhibition of BCL-W and BCL-XL., Nat. Commun. 7 (2016) 11190. https://doi.org/10.1038/ncomms11190.

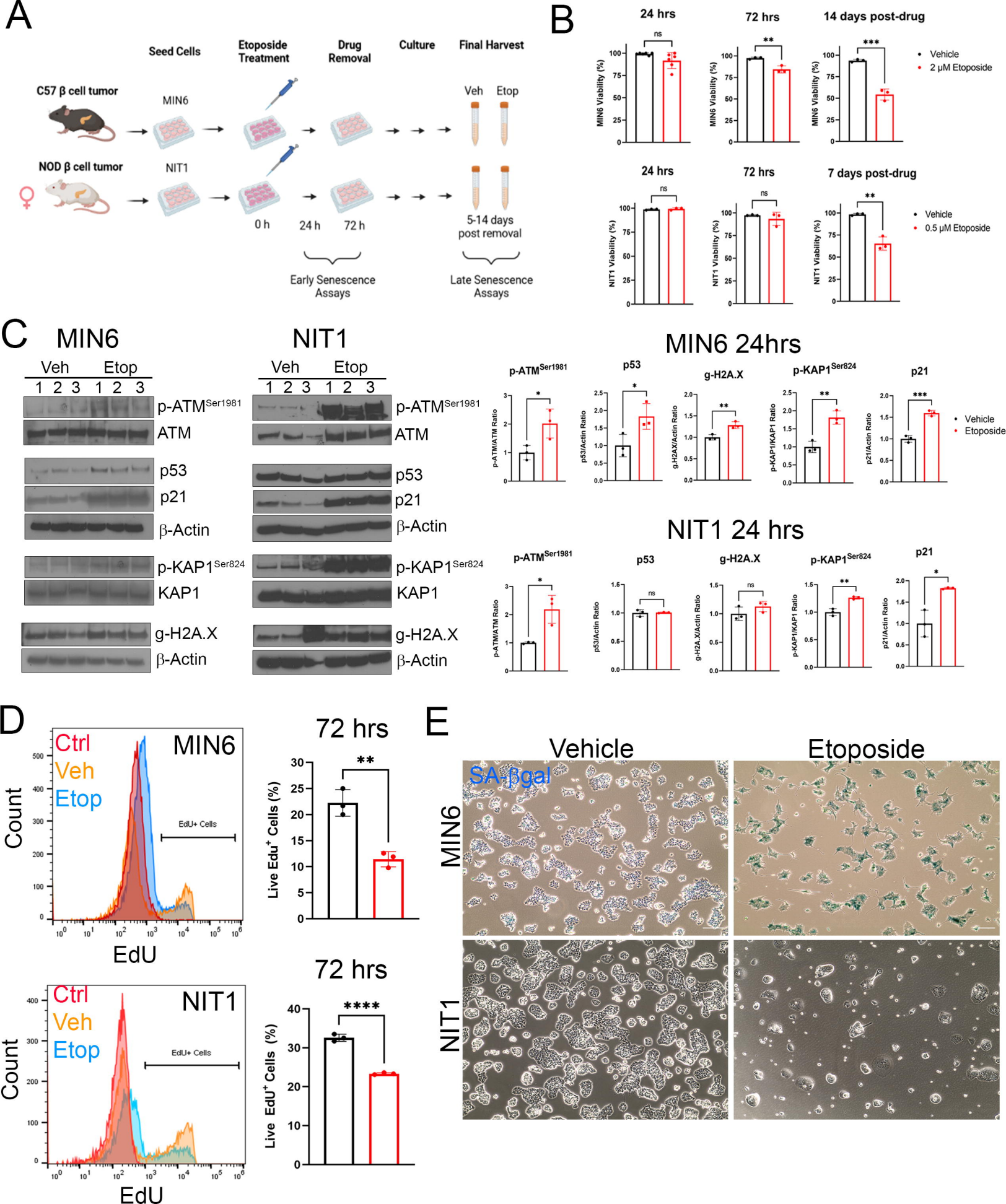
A
Seed Cells
Etoposide Treatment
Drug Removal
Culture
Final Harvest
C57 β cell tumor
MIN6
Veh
Etop
NOD β cell tumor
NIT1
0 h
24 h
72 h
5-14 days post removal
Early Senescence Assays
Late Senescence Assays
B
24 hrs
72 hrs
14 days post-drug
MIN6 Viability (%)
Vehicle
2 μM Etoposide
7 days post-drug
NIT1 Viability (%)
0.5 μM Etoposide
C
MIN6
NIT1
Veh
Etop
p-ATM Ser1981
ATM
p53
p21
β-Actin
p-KAP1 Ser824
KAP1
g-H2A.X
MIN6 24hrs
NIT1 24 hrs
p-ATM/ATM Ratio
p53/Actin Ratio
g-H2AX/Actin Ratio
p-KAP1/KAP1 Ratio
p21/Actin Ratio
Vehicle
Etoposide
D
Ctrl
Veh
Etop
MIN6
NIT1
EdU+ Cells
Count
EdU
72 hrs
Live EdU+ Cells (%)
E
Vehicle
Etoposide
SA-βgal
MIN6
NIT1

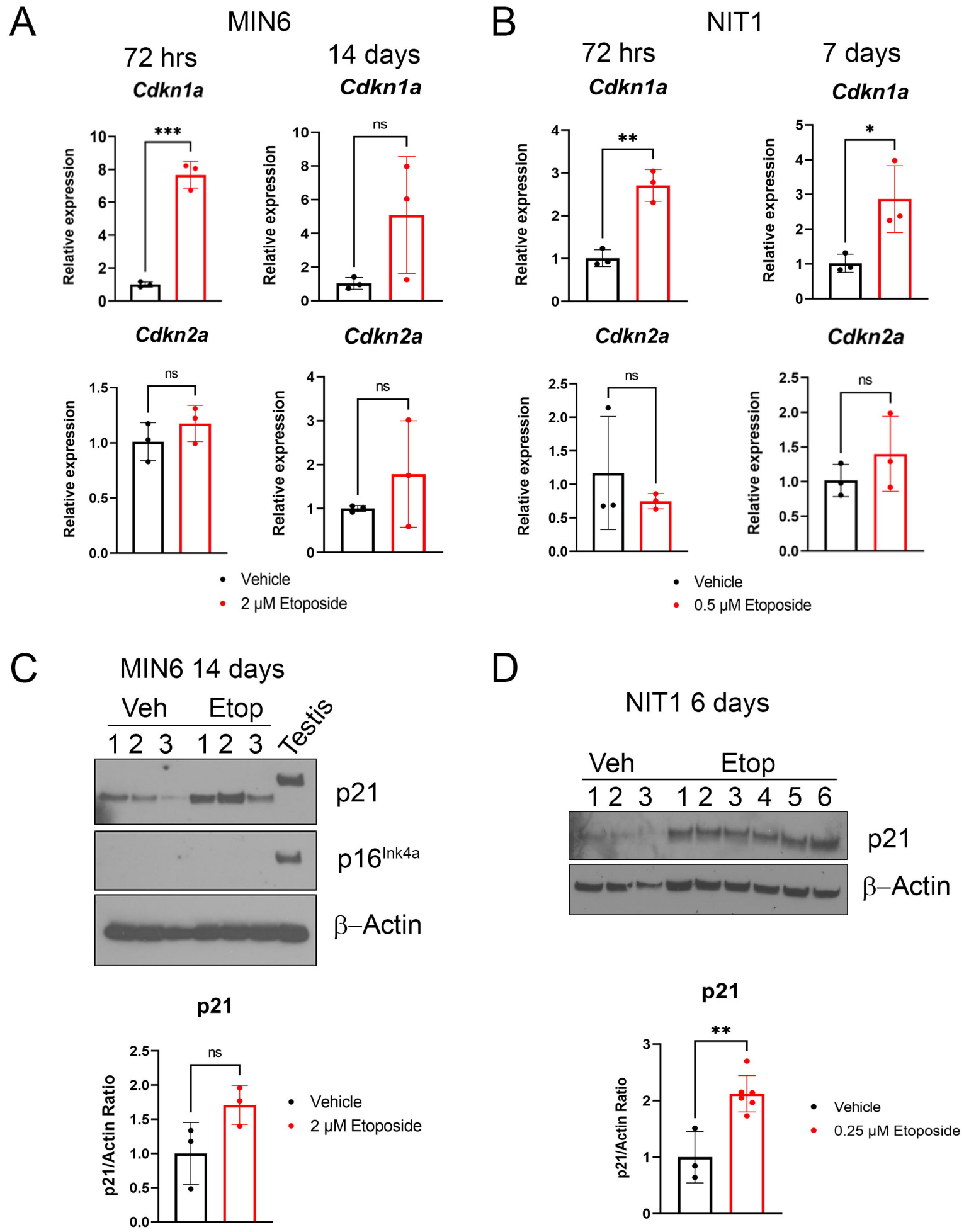
A
MIN6
72 hrs
14 days
Cdkn1a
Cdkn2a
Relative expression
***
ns
Vehicle
2 μM Etoposide
B
NIT1
72 hrs
7 days
**
*
0.5 μM Etoposide
C
MIN6 14 days
Veh
Etop
1 2 3 1 2 3
Testis
p21
p16Ink4a
β–Actin
p21/Actin Ratio
D
NIT1 6 days
1 2 3 1 2 3 4 5 6
0.25 μM Etoposide

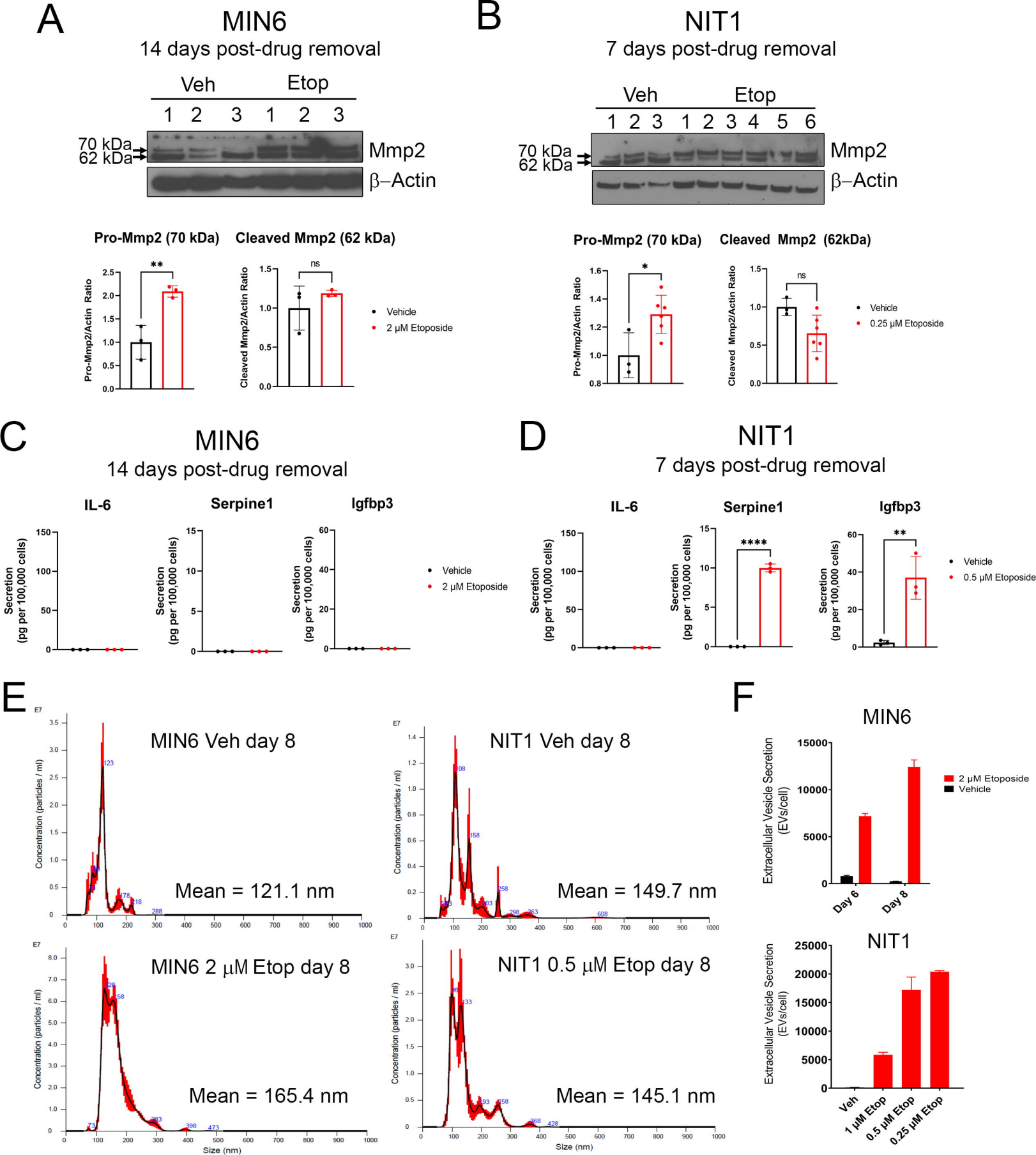
A
MIN6
14 days post-drug removal
Veh
Etop
1 2 3 1 2 3
70 kDa
62 kDa
Mmp2
β–Actin
Pro-Mmp2 (70 kDa)
Cleaved Mmp2 (62 kDa)
Pro-Mmp2/Actin Ratio
Cleaved Mmp2/Actin Ratio
**
ns
Vehicle
2 μM Etoposide
B
NIT1
7 days post-drug removal
Veh
Etop
1 2 3 1 2 3 4 5 6
70 kDa
62 kDa
Mmp2
β–Actin
Pro-Mmp2 (70 kDa)
Cleaved Mmp2 (62kDa)
Pro-Mmp2/Actin Ratio
Cleaved Mmp2/Actin Ratio
*
ns
Vehicle
0.25 μM Etoposide
C
MIN6
14 days post-drug removal
IL-6
Serpine1
Igfbp3
Secretion (pg per 100,000 cells)
Vehicle
2 μM Etoposide
D
NIT1
7 days post-drug removal
IL-6
Serpine1
Igfbp3
Secretion (pg per 100,000 cells)
****
**
Vehicle
0.5 μM Etoposide
E
MIN6 Veh day 8
Mean = 121.1 nm
NIT1 Veh day 8
Mean = 149.7 nm
MIN6 2 μM Etop day 8
Mean = 165.4 nm
NIT1 0.5 μM Etop day 8
Mean = 145.1 nm
Concentration (particles / ml)
Size (nm)
F
MIN6
Extracellular Vesicle Secretion (EVs/cell)
2 μM Etoposide
Vehicle
Day 6
Day 8
NIT1
Extracellular Vesicle Secretion (EVs/cell)
Veh
1 μM Etop
0.5 μM Etop
0.25 μM Etop

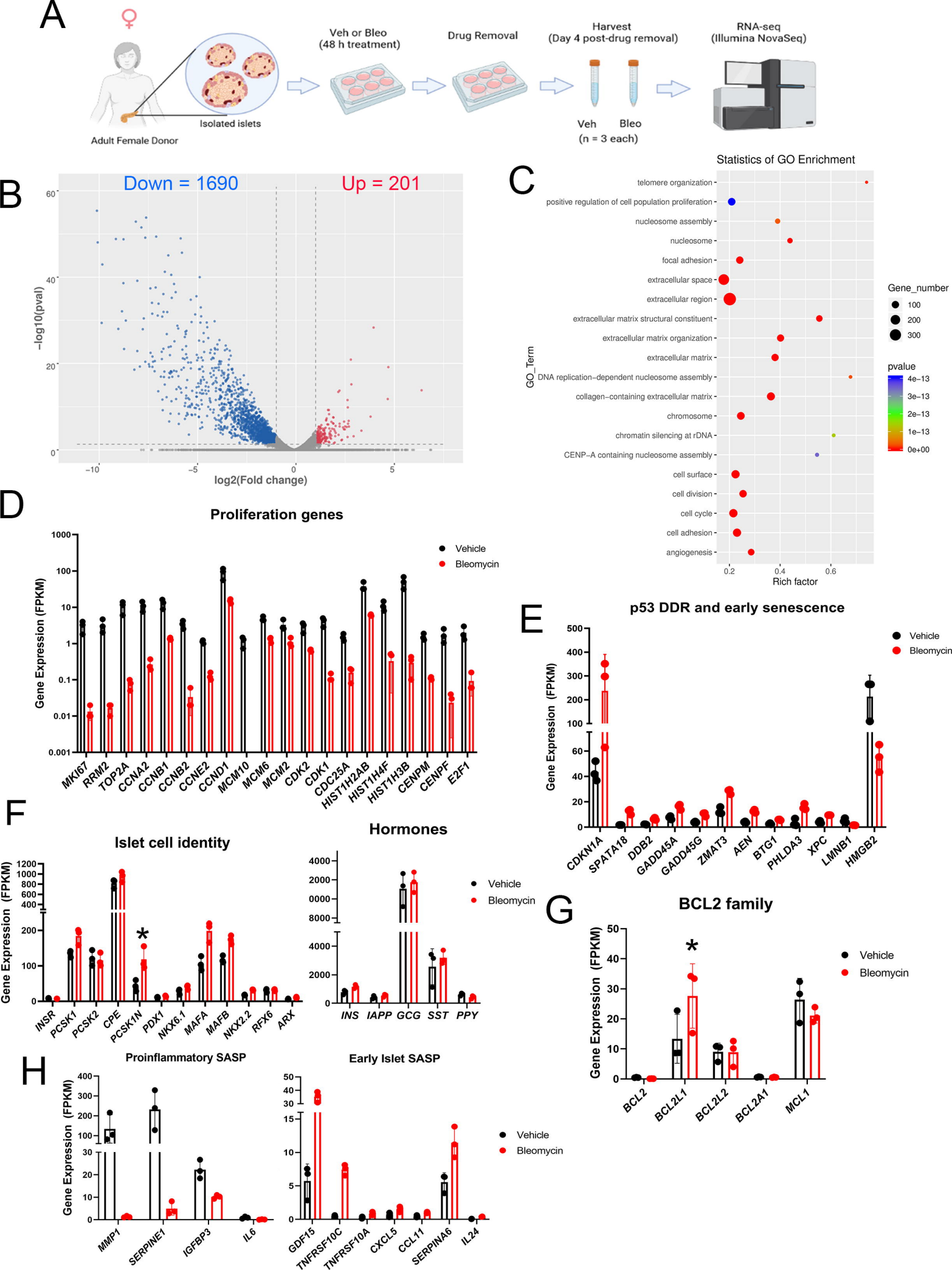
A
Adult Female Donor
Isolated islets
Veh or Bleo
(48 h treatment)
Drug Removal
Harvest
(Day 4 post-drug removal)
RNA-seq
(Illumina NovaSeq)
Veh
Bleo
(n = 3 each)
B
Down = 1690
Up = 201
−log10(pval)
log2(Fold change)
C
Statistics of GO Enrichment
GO_Term
telomere organization
positive regulation of cell population proliferation
nucleosome assembly
nucleosome
focal adhesion
extracellular space
extracellular region
extracellular matrix structural constituent
extracellular matrix organization
extracellular matrix
DNA replication−dependent nucleosome assembly
collagen−containing extracellular matrix
chromosome
chromatin silencing at rDNA
CENP−A containing nucleosome assembly
cell surface
cell division
cell cycle
cell adhesion
angiogenesis
Rich factor
Gene_number
pvalue
D
Proliferation genes
Gene Expression (FPKM)
Vehicle
Bleomycin
MKI67
RRM2
TOP2A
CCNA2
CCNB1
CCNB2
CCNE2
CCND1
MCM10
MCM6
MCM2
CDK2
CDK1
CDC25A
HIST1H2AB
HIST1H4F
HIST1H3B
CENPM
CENPF
E2F1
E
p53 DDR and early senescence
Gene Expression (FPKM)
Vehicle
Bleomycin
CDKN1A
SPATA18
DDB2
GADD45A
GADD45G
ZMAT3
AEN
BTG1
PHLDA3
XPC
LMNB1
HMGB2
F
Islet cell identity
Gene Expression (FPKM)
INSR
PCSK1
PCSK2
CPE
PCSK1N
PDX1
NKX6.1
MAFA
MAFB
NKX2.2
RFX6
ARX
Hormones
INS
IAPP
GCG
SST
PPY
Vehicle
Bleomycin
G
BCL2 family
Gene Expression (FPKM)
BCL2
BCL2L1
BCL2L2
BCL2A1
MCL1
Vehicle
Bleomycin
H
Proinflammatory SASP
Gene Expression (FPKM)
MMP1
SERPINE1
IGFBP3
IL6
Early Islet SASP
GDF15
TNFRSF10C
TNFRSF10A
CXCL5
CCL11
SERPINA6
IL24
Vehicle
Bleomycin